JACS
JOURNAL OF THE AMERICAN CHEMICAL SOCIETY

pubs.acs.org/JACS

Communication

Narcissistic, Integrative, and Kinetic Self-Sorting within a System of Coordination Cages

Felix. J. Rizzuto and Jonathan R. Nitschke*

Cite This: *J. Am. Chem. Soc.* 2020, 142, 7749–7753

Read Online

ACCESS | Metrics & More | Article Recommendations | Supporting Information

ABSTRACT: Many useful principles of self-assembly have been elucidated through studies of systems where multiple components combine to create a single structure. More complex systems, where multiple product structures self-assemble in parallel from a shared set of precursors, are also of great interest, as biological systems exhibit this behavior. The greater complexity of such systems leads to an increased likelihood that discrete species will not be formed, however. Here we show how the kinetics of self-assembly govern the formation of multiple metal−organic architectures from a mixture of five building blocks, preventing the formation of a discrete structure of intermediate size. By varying ligand symmetry, denticity, and orientation, we explore how five distinct polyhedra—a tetrahedron, an octahedron, a cube, a cuboctahedron, and a triangular prism—assemble in concert around Co^{II} template ions. The underlying rules dictating the organization of assemblies into specific shapes are deciphered, explaining the formation of only three discrete entities when five could form in principle.

Molecules may follow complex pathways during self-assembly processes that generate multiple products. Understanding the self-sorting processes that occur within these pathways may allow us to decipher how simple prebiotic chemicals developed into life,[1−3] and also how to design synthetic chemical systems that may be of practical use.[4−14]

When different molecules self-assemble, one of three outcomes may result: *social* sorting,[15,16] where a statistical distribution of products is observed, *narcissistic* sorting,[17−19] where components self-recognize and generate homoleptic architectures, or *integrative* self-sorting,[20−24] during which all components are assimilated into a single product. Other sorting modes have recently been discovered, including biased sorting regimes[25] and those driven by kinetic trapping,[26] stereochemical differences,[27,28] or template-induced sorting.[29]

Metal−organic cages have displayed a wealth of sorting behaviors that can be understood in terms of thermodynamic and geometric parameters.[30−35] We hypothesized that combinations of ligands with different denticities and symmetries would yield complex, but potentially predictable sorting behavior. We thus explored the sorting characteristics of three- and fourfold symmetric polyamine subcomponents with bidentate and tridentate aldehyde subcomponents, using Co^{II} as the metal ion template during subcomponent self-assembly.

Four polyhedral coordination cages were prepared using Co^{II} as a template ion, as shown in Figure 1, and as described in Supporting Information (SI) Section 2. Tritopic **A** and tetratopic **B** thus generated threefold and fourfold symmetry axes, respectively, and 2-formylpyridine **P1** and 2-formylphenanthroline **P2** created bidentate and tridentate coordination sites upon condensation with these two polyamines, allowing the Co^{II} centers to serve as three- or twofold symmetry axes. The relative orientations of these ligand- and metal-generated symmetry elements thus brought about the geometries of $Co^{II}_4L_4$ tetrahedron **1**, $Co^{II}_6L_4$ octahedron **2**, $Co^{II}_8L_6$ cube **3**, and $Co^{II}_{12}L_6$ cuboctahedron **4**.[25,29,36,37]

When two different polyamines self-assemble with a single aldehyde, possible outcomes include narcissistic and integrative self-sorting. When tetratopic and tritopic amines **B** and **C** reacted with aldehyde **P1** and Co^{II} (Figure 2a), both narcissistic and integrative processes were observed to occur in parallel. The narcissistically sorted cube **3** and tetrahedron **5** were thus observed to form in equilibrium with the integrative product **6**, a heteroleptic trigonal prism containing two residues of **C** and three of **B** (SI Section 3.3.2). The structure of **6** (Figure 2b) is similar to that of a reported analog,[21] although the free base porphyrin faces of **6** do not adapt the inward- and outward-facing conformations observed for their Ni^{II}-centered congeners.[21]

When both aldehydes **P1** and **P2** reacted with Co^{II} and either amine **A** or **B**, clean narcissistic self-sorting was observed (Figure 3a, SI Sections 3.1 and 3.2). Tritopic **A** produced **1** and **2**, and tetratopic **B** produced **3** and **4**, with product ratios depending on the amounts of **P1** and **P2** used initially.[38]

Different behavior was observed when only one of the aldehyde subcomponents **P1** or **P2** reacted with both amine subcomponents **A** and **B** and Co^{II} (Figure 3b). When triamine **A** and tetramine **B** were combined with 2-formylpyridine **P1** in a 1:1 mixture of DMF/MeCN, only tetrahedron **1** and cube **3** were observed (Figures S14, S15). However, when pure MeCN was used as the reaction solvent, a third product **7** was

Received: March 2, 2020
Published: April 10, 2020

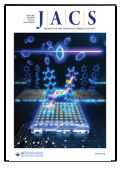

https://dx.doi.org/10.1021/jacs.0c02444
J. Am. Chem. Soc. 2020, 142, 7749–7753

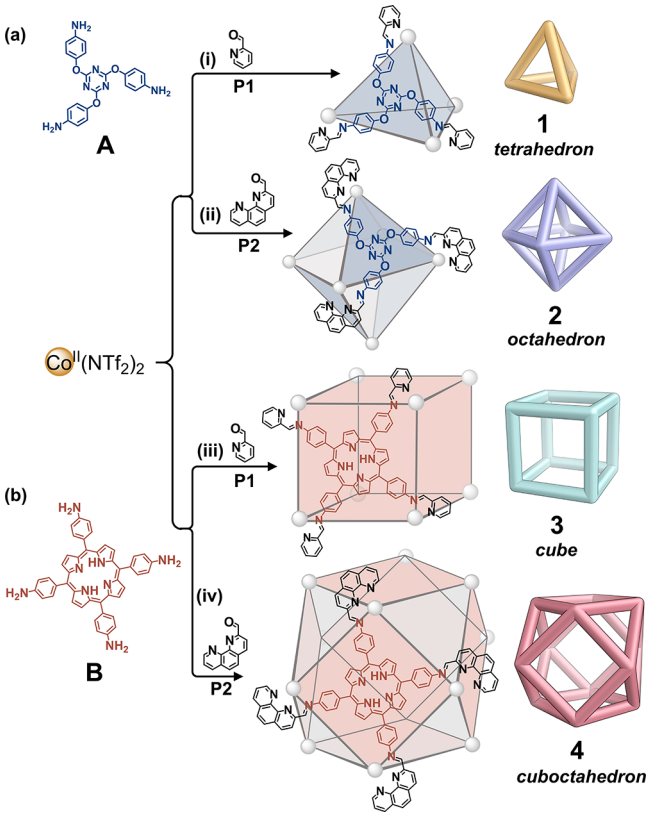

Figure 1. Four different architectures can be synthesized by Co^{II}-templated imine condensation of amine **A** or **B** with aldehyde **P1** or **P2**. (a) Threefold symmetric subcomponent **A** generated (i) $Co^{II}_4L_4$ tetrahedron **1** and (ii) $Co^{II}_6L_4$ octahedron **2**. (b) Fourfold symmetric subcomponent **B** generated (iii) $Co^{II}_8L_6$ cube **3** and (iv) $Co^{II}_{12}L_6$ cuboctahedron **4**. Lines connect nearest-neighbor metal ions.

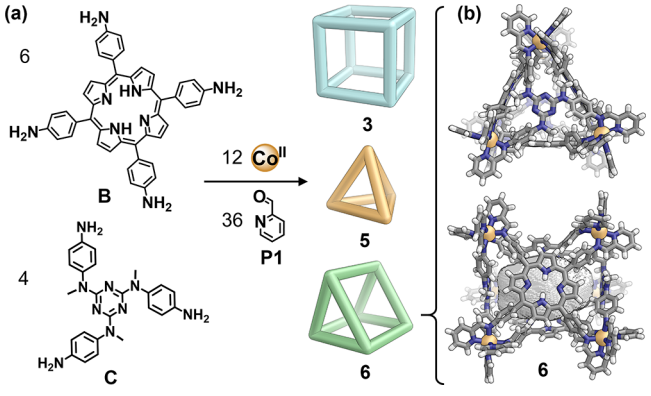

Figure 2. (a) Subcomponents **B** and **C** underwent both narcissistic self-sorting to produce a mixture of cube **3** (from **B**) and tetrahedron **5** (from **C**), and integrative self-assembly to produce trigonal prism **6**, which incorporates both **B** and **C**. Product ratios were determined to be 23% cube **3**, 51% triangular prism **6**, and 26% tetrahedron **5** by ^{1}H NMR integration. (b) X-ray crystal structure of **6**, viewed facing the tritopic (top) and tetratopic (bottom) ligands. The void space inside the structure is displayed as a gray solid (Co, orange; C, gray; N, blue; H, white).

also observed by ESI-MS (Figure S17). Product **7** incorporates three residues of **B** and two of **A**, and we infer it to have a similar trigonal-prismatic framework to structurally characterized **6** (Figure 2b).

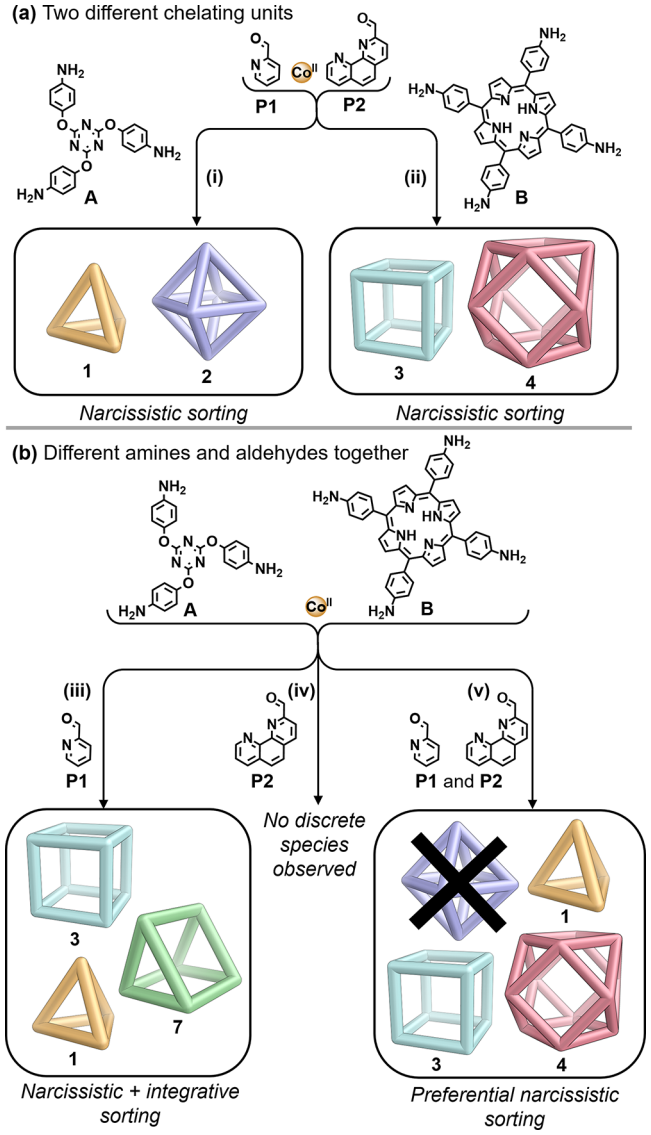

Figure 3. (a) Narcissistic self-sorting was observed when the two aldehyde subcomponents **P1** and **P2** were both employed with either (i) **A** or (ii) **B** during self-assembly. (b) More complex outcomes resulted from the self-assembly of both amines **A** and **B** with either or both of the aldehydes. (iii) **A**, **B**, and **P1** combined to form homoleptic **1** and **3** and heteroleptic **7**. (iv) **A**, **B**, and **P2** yielded no discrete products, and (v) **A**, **B**, **P1**, and **P2** gave **1**, **3**, and **4**.

The combination of amines **A** and **B** with 2-formylphenanthroline **P2** (Figure 3b, pathway (iv)) resulted in a mixture of products that gave a complex NMR spectrum (Figure S21) that did not display peaks corresponding to any isolated discrete product. Multiple different products may thus form, integrating both **A** and **B**, without a strong thermodynamic preference for any single outcome. The lack of narcissistic sorting of octahedron **2** and cuboctahedron **4** may also contribute to the lack of observation of the former species in the five-component sorting experiment described below.

When all five building blocks (**A**, **B**, Co^{II}, **P1**, and **P2**) were combined in the correct ratio so as to allow an equimolar mixture of cages **1**:**2**:**3**:**4** to form, octahedron **2** was not observed to form (Figure 3b, pathway (v)). Instead, tetrahedron **1**, cube **3**, and cuboctahedron **4** were the only species observed by both ^{1}H NMR (Figure 4) and ESI-MS

https://dx.doi.org/10.1021/jacs.0c02444
J. Am. Chem. Soc. 2020, 142, 7749−7753

(Figure S24). Monitored over 3 days of heating, **2** was not observed to form at any time (Figure S25).

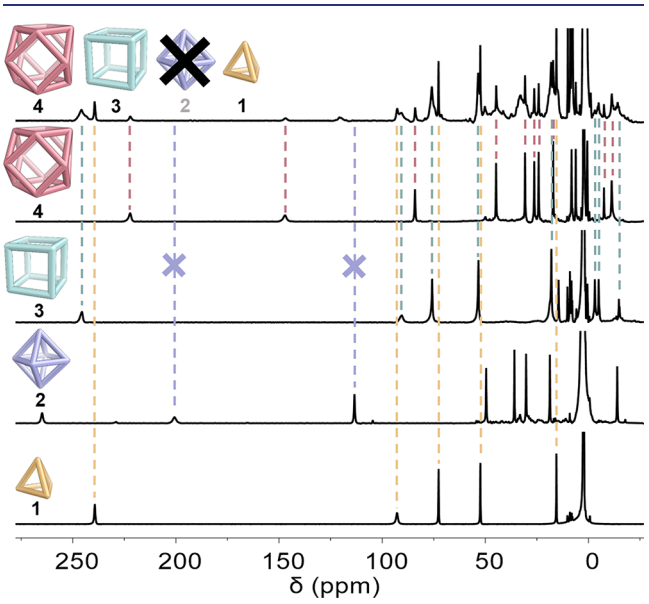

Figure 4. ^{1}H NMR spectra (400 MHz, 298 K, CD_3CN) of each separate cage (bottom four spectra) compared to the mixture generated (Figure 3b, pathway (v)) when **A**, **B**, **P1**, and **P2** were mixed with Co^{II} (topmost spectrum).

In contrast with reported systems,[38,39] the mixtures of products obtained in the system of Figure 3b, pathway (v) is not determined uniquely by the stoichiometry of subcomponents employed.[38] A subset of only two or three of the four cages (**1**, **2**, **3**, **4**) will be able to consume all of a balanced set of building blocks, i.e., where the total number of aldehyde groups is equal to the total number of amine groups, and where all Co^{II} is coordinatively saturated. Thus, the selectivity observed when all subcomponents are present together (Figure 3b, pathway (v)) must be a result of further factors acting upon the system.

The rates of formation of the four cages were gauged, as shown in Figure 5. At regular intervals during self-assembly at 60 °C, we extracted aliquots and measured the degree of completion of assembly by UV−vis spectroscopy (SI Section 4). For all cages, we monitored the evolution of MLCT transitions (which often overlapped with ligand $\pi \rightarrow \pi^*$ transitions, and porphyrin Soret bands in the cases of **3** and **4**) as a function of time. A plateau in the intensity of the absorbance marked complete formation of the cage, which was then verified by ^{1}H NMR spectroscopy. As the assembly kinetics of these structures are complex, we fitted our data to a simple exponential rate equation, enabling a comparison of assembly half-lives between cages.

The data of Figure 5 show clear differences between the rates of formation of the four structures. Tetrahedron **1** forms most rapidly, followed by octahedron **2**, cube **3**, and cuboctahedron **4**. This sequence reflects the increasing structural complexity of these assemblies.

These rate differences (Figure 5) shed light upon the selectivity exhibited by the system of Figure 3b, pathway (v), as shown in Figure 6. As tetrahedron **1** forms most rapidly, it consumes all of the **A** and most of the **P1** from the initial mixture. The remaining **P1** must react with **B** to form cube **3**,

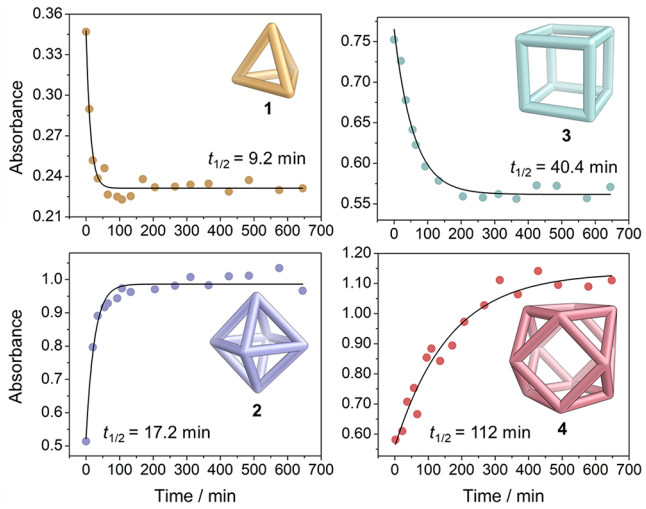

Figure 5. Plots showing the rate of formation of each homoleptic architecture, monitored by UV−vis spectroscopy, following the principal optical bands of **1** (346 nm) and **2** (370 nm), and the MLCT transitions of **3** (430 nm) and **4** (445 nm), which overlapped with porphyrin Soret bands. Black lines represent the best fits to an exponential rate equation (Absorbance = $A_0 + Ae^{\lambda t}$), from which $t_{1/2} = \ln 2/\lambda$.

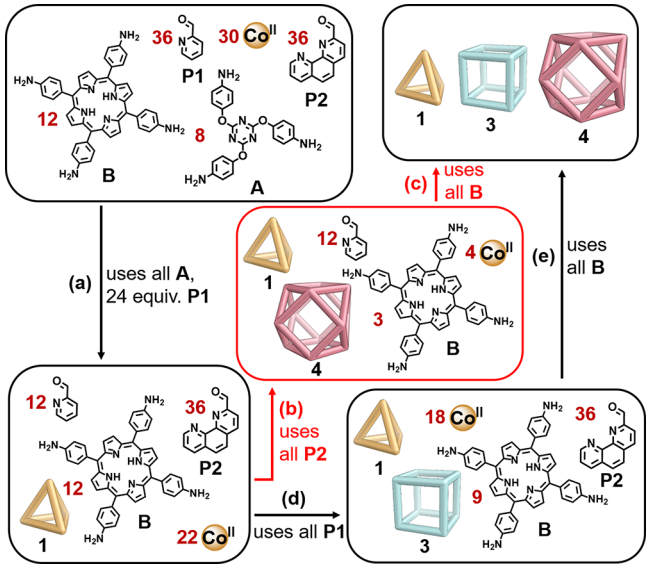

Figure 6. An outline of the process inferred to occur when **A**, **B**, **P1**, **P2**, and Co^{II} are mixed in the proportions shown. (a) Tetrahedron **1** forms first, sequestering all **A**. (b) Cuboctahedron **4** may then form, consuming all **P2**, followed by (c) cube **3**, or else (d) cube **3** may form first, consuming all **P1**, followed by cuboctahedron **4**. Both paths lead to an identical final state in which only **1**, **3**, and **4** are observed.

leaving additional **B** to react with the **P2** to form cuboctahedron **4**. Structures **3** and **4** may form in either order, as the system becomes deterministic[38] following the conversion of all **A** into **1**, with only one fate possible for each of the remaining subcomponents. The relative rates of **3** and **4** formation (Figure 5) suggest that **3** will be formed ahead of **4**, however.

The first structure to form, tetrahedron **1**, thus sets the scene for the system's subsequent self-assembly by preferentially consuming all of **A** that octahedron **2** would have otherwise required. This system appears quite sensitive to subtle effects,

https://dx.doi.org/10.1021/jacs.0c02444
J. Am. Chem. Soc. 2020, 142, 7749−7753

given the relatively small (less than a factor of 2) difference between the formation times of the competing structures **1** and **2**. Notably, **2** was never observed when different reactant stoichiometries were employed during the reaction described in Figure 3b, pathway (v) (Figures S26–28).

Host–guest binding can influence the kinetics of cage formation.[40,41] This study thus lays the foundations to direct the self-assembly of systems of cages that share building blocks through the addition of guests, and other "cofactors" whose influence on one component of the system may propagate through its entirety, amplifying certain structures and suppressing others. In systems where cages are serving useful functions, such as catalysis[42,43] or cargo transport,[44,45] such an understanding may allow the development of these functions to be programmed in a complex way from a simple set of input stimuli.

■ ASSOCIATED CONTENT

Supporting Information

The Supporting Information is available free of charge at https://pubs.acs.org/doi/10.1021/jacs.0c02444.

Syntheses of cages, sorting experiments, crystallographic details (PDF)

CIF for **6** (CCDC 1962805) (CIF)

■ AUTHOR INFORMATION

Corresponding Author

Jonathan R. Nitschke − *University of Cambridge, Department of Chemistry, Cambridge CB2 1EW, U.K.;* orcid.org/0000-0002-4060-5122; Email: jrn34@cam.ac.uk

Author

Felix. J. Rizzuto − *University of Cambridge, Department of Chemistry, Cambridge CB2 1EW, U.K.;* orcid.org/0000-0003-2799-903X

Complete contact information is available at: https://pubs.acs.org/10.1021/jacs.0c02444

Notes

The authors declare no competing financial interest.

■ ACKNOWLEDGMENTS

This work was supported by the UK Engineering and Physical Sciences Research Council (EPSRC, EP/P027067/1). F.J.R. thanks Cambridge Australia Scholarships for Ph.D. funding. We thank Diamond Light Source for time on beamline I19 (MT-11397).

■ REFERENCES

(1) Altay, M.; Altay, Y.; Otto, S. Parasitic Behavior of Self-Replicating Molecules. *Angew. Chem., Int. Ed.* **2018**, *57*, 10564–10568.

(2) Altay, Y.; Tezcan, M.; Otto, S. Emergence of a New Self-Replicator from a Dynamic Combinatorial Library Requires a Specific Pre-Existing Replicator. *J. Am. Chem. Soc.* **2017**, *139*, 13612–13615.

(3) Luisi, P. L. Chemistry Constraints on the Origin of Life. *Isr. J. Chem.* **2015**, *55*, 906–918.

(4) Safont-Sempere, M. M.; Fernández, G.; Würthner, F. Self-Sorting Phenomena in Complex Supramolecular Systems. *Chem. Rev.* **2011**, *111*, 5784–5814.

(5) Lehn, J.-M. Toward complex matter: Supramolecular chemistry and self-organization. *Proc. Natl. Acad. Sci. U. S. A.* **2002**, *99*, 4763–4768.

(6) Northrop, B. H.; Zheng, Y.-R.; Chi, K.-W.; Stang, P. J. Self-Organization in Coordination-Driven Self-Assembly. *Acc. Chem. Res.* **2009**, *42*, 1554–1563.

(7) Hsu, C.-W.; Miljanïc, O. Š. Adsorption-Driven Self-Sorting of Dynamic Imine Libraries. *Angew. Chem.* **2015**, *127*, 2247–2250.

(8) Vantomme, G.; Meijer, E. W. The construction of supramolecular systems. *Science* **2019**, *363*, 1396–1397.

(9) Hou, X.; Ke, C.; Bruns, C. J.; McGonigal, P. R.; Pettman, R. B.; Stoddart, J. F. Tunable solid-state fluorescent materials for supramolecular encryption. *Nat. Commun.* **2015**, *6*, 6884.

(10) Spengler, M.; Dong, R. Y.; Michal, C. A.; Hamad, W. Y.; MacLachlan, M. J.; Giese, M. Hydrogen-Bonded Liquid Crystals in Confined Spaces - Toward Photonic Hybrid Materials. *Adv. Funct. Mater.* **2018**, *28*, 1800207.

(11) Aβhoff, S. J.; Sukas, S.; Yamaguchi, T.; Hommersom, C. A.; Le Gac, S.; Katsonis, N. Superstructures of chiral nematic microspheres as all-optical switchable distributors of light. *Sci. Rep.* **2015**, *5*, 14183.

(12) Krieg, E.; Niazov-Elkan, A.; Cohen, E.; Tsarfati, Y.; Rybtchinski, B. Noncovalent Aqua Materials Based on Perylene Diimides. *Acc. Chem. Res.* **2019**, *52*, 2634–2646.

(13) Karalius, A.; Zhang, Y.; Kravchenko, O.; Elofsson, U.; Szabó, Z.; Yan, M.; Ramström, O. Formation and Out-of-Equilibrium, High/Low State Switching of a Nitroaldol Dynamer in Neutral Aqueous Media. *Angew. Chem., Int. Ed.* **2020**, *59*, 3434.

(14) Septavaux, J.; Tosi, C.; Jame, P.; Nervi, C.; Gobetto, R.; Leclaire, J. Simultaneous CO_2 capture and metal purification from waste streams using triple-level dynamic combinatorial chemistry. *Nat. Chem.* **2020**, *12*, 202–212.

(15) Li, J.; Nowak, P.; Otto, S. Dynamic Combinatorial Libraries: From Exploring Molecular Recognition to Systems Chemistry. *J. Am. Chem. Soc.* **2013**, *135*, 9222–9239.

(16) Black, S. P.; Sanders, J. K. M.; Stefankiewicz, A. R. Disulfide exchange: exposing supramolecular reactivity through dynamic covalent chemistry. *Chem. Soc. Rev.* **2014**, *43*, 1861–1872.

(17) Beaudoin, D.; Rominger, F.; Mastalerz, M. Chiral Self-Sorting of [2 + 3] Salicylimine Cage Compounds. *Angew. Chem., Int. Ed.* **2017**, *56*, 1244–1248.

(18) Zheng, K.; Wang, H.; Chow, H.-F. Organogelating and narcissistic self-sorting behaviour of non-preorganized oligoamides. *Chem. Sci.* **2019**, *10*, 4015–4024.

(19) Acharyya, K.; Mukherjee, S.; Mukherjee, P. S. Molecular Marriage through Partner Preferences in Covalent Cage Formation and Cage-to-Cage Transformation. *J. Am. Chem. Soc.* **2013**, *135*, 554–557.

(20) He, Z.; Jiang, W.; Schalley, C. A. Integrative self-sorting: a versatile strategy for the construction of complex supramolecular architecture. *Chem. Soc. Rev.* **2015**, *44*, 779–789.

(21) Rizzuto, F. J.; Carpenter, J. P.; Nitschke, J. R. Multisite Binding of Drugs and Natural Products in an Entropically Favorable, Heteroleptic Receptor. *J. Am. Chem. Soc.* **2019**, *141*, 9087–9095.

(22) Chen, B.; Holstein, J. J.; Horiuchi, S.; Hiller, W. G.; Clever, G. H. Pd(II) Coordination Sphere Engineering: Pyridine Cages, Quinoline Bowls, and Heteroleptic Pills Binding One or Two Fullerenes. *J. Am. Chem. Soc.* **2019**, *141*, 8907–8913.

(23) Cirulli, M.; Kaur, A.; Lewis, J. E. M.; Zhang, Z.; Kitchen, J. A.; Goldup, S. M.; Roessler, M. M. Rotaxane-Based Transition Metal Complexes: Effect of the Mechanical Bond on Structure and Electronic Properties. *J. Am. Chem. Soc.* **2019**, *141*, 879–889.

(24) Schmittel, M.; Saha, S. Chapter Three - From Self-Sorting of Dynamic Metal-Ligand Motifs to (Supra)Molecular Machinery in Action. *Adv. Inorg. Chem.* **2018**, *71*, 135–175.

(25) Rizzuto, F. J.; Kieffer, M.; Nitschke, J. R. Quantified structural speciation in self-sorted $Co^{II}{}_6L_4$ cage systems. *Chem. Sci.* **2018**, *9*, 1925–1930.

(26) Yan, Y.; Huang, J.; Tang, B. Z. Kinetic trapping − a strategy for directing the self-assembly of unique functional nanostructures. *Chem. Commun.* **2016**, *52*, 11870–11884.

(27) Zhong, J.; Zhang, L.; August, D. P.; Whitehead, G. F. S.; Leigh, D. A. Self-Sorting Assembly of Molecular Trefoil Knots of Single Handedness. *J. Am. Chem. Soc.* **2019**, *141*, 14249−14256.
(28) Tateishi, T.; Kojima, T.; Hiraoka, S. Chiral self-sorting process in the self-assembly of homochiral coordination cages from axially chiral ligands. *Commun. Chem.* **2018**, *1*, 20.
(29) Rizzuto, F. J.; Nitschke, J. R. Stereochemical plasticity modulates cooperative binding in a $CoII_{12}L_6$ cuboctahedron. *Nat. Chem.* **2017**, *9*, 903−908.
(30) Holloway, L. R.; Bogie, P. M.; Hooley, R. J. Controlled self-sorting in self-assembled cage complexes. *Dalton Trans.* **2017**, *46*, 14719−14723.
(31) Fujita, D.; Ueda, Y.; Sato, S.; Mizuno, N.; Kumasaka, T.; Fujita, M. Self-assembly of tetravalent Goldberg polyhedra from 144 small components. *Nature* **2016**, *540*, 563−566.
(32) Caulder, D. L.; Brückner, C.; Powers, R. E.; König, S.; Parac, T. N.; Leary, J. A.; Raymond, K. N. Design, Formation and Properties of Tetrahedral M_4L_4 and M_4L_6 Supramolecular Clusters. *J. Am. Chem. Soc.* **2001**, *123*, 8923−8938.
(33) Rizzuto, F. J.; von Krbek, L. K. S.; Nitschke, J. R. Strategies for binding multiple guests in metal-organic cages. *Nat. Rev. Chem.* **2019**, *3*, 204−222.
(34) Chakraborty, S.; Newkome, G. R. Terpyridine-based metallosupramolecular constructs: tailored monomers to precise 2D-motifs and 3D-metallocages. *Chem. Soc. Rev.* **2018**, *47*, 3991−4016.
(35) Frank, M.; Krause, L.; Herbst-Irmer, R.; Stalke, D.; Clever, G. H. Narcissistic self-sorting vs. statistic ligand shuffling within a series of phenothiazine-based coordination cages. *Dalton Trans.* **2014**, *43*, 4587−4592.
(36) Ferguson, A.; Staniland, R. W.; Fitchett, C. M.; Squire, M. A.; Williamson, B. E.; Kruger, P. E. Variation of guest selectivity within $[Fe_4L_4]^{8+}$ tetrahedral cages through subtle modification of the face-capping ligand. *Dalton Trans.* **2014**, *43*, 14550−14553.
(37) Meng, W.; Breiner, B.; Rissanen, K.; Thoburn, J. D.; Clegg, J. K.; Nitschke, J. R. A Self-Assembled M_8L_6 Cubic Cage that Selectively Encapsulates Large Aromatic Guests. *Angew. Chem., Int. Ed.* **2011**, *50*, 3479−3483.
(38) Sarma, R. J.; Nitschke, J. R. Self-Assembly in Systems of Subcomponents: Simple Rules, Subtle Consequences. *Angew. Chem., Int. Ed.* **2008**, *47*, 377−380.
(39) Ayme, J.-F.; Lehn, J.-M. Self-sorting of two imine-based metal complexes: balancing kinetics and thermodynamics in constitutional dynamic networks. *Chem. Sci.* **2020**, *11*, 1114−1121.
(40) Hall, B. R.; Manck, L. E.; Tidmarsh, I. S.; Stephenson, A.; Taylor, B. F.; Blaikie, E. J.; Griend, D. A. V.; Ward, M. D. Structures, host-guest chemistry and mechanism of stepwise self-assembly of M4L6 tetrahedral cage complexes. *Dalton Trans.* **2011**, *40*, 12132−12145.
(41) Paul, R. L.; Bell, Z. R.; Jeffery, J. C.; McCleverty, J. A.; Ward, M. D. Anion-templated self-assembly of tetrahedral cage complexes of cobalt(II) with bridging ligands containing two bidentate pyrazolyl-pyridine binding sites. *Proc. Natl. Acad. Sci. U. S. A.* **2002**, *99*, 4883−4888.
(42) Fang, Y.; Powell, J. A.; Li, E.; Wang, Q.; Perry, Z.; Kirchon, A.; Yang, X.; Xiao, Z.; Zhu, C.; Zhang, L.; Huang, F.; Zhou, H.-C. Catalytic reactions within the cavity of coordination cages. *Chem. Soc. Rev.* **2019**, *48*, 4707−4730.
(43) Brown, C. J.; Toste, F. D.; Bergman, R. G.; Raymond, K. N. Supramolecular Catalysis in Metal-Ligand Cluster Hosts. *Chem. Rev.* **2015**, *115*, 3012−3035.
(44) Grancha, T.; Carné-Sánchez, A.; Hernández-López, L.; Albalad, J.; Imaz, I.; Juanhuix, J.; Maspoch, D. Phase Transfer of Rhodium(II)-Based Metal-Organic Polyhedra Bearing Coordinatively Bound Cargo Enables Molecular Separation. *J. Am. Chem. Soc.* **2019**, *141*, 18349−18355.
(45) Grommet, A. B.; Hoffman, J. B.; Percástegui, E. G.; Mosquera, J.; Howe, D. J.; Bolliger, J. L.; Nitschke, J. R. Anion Exchange Drives Reversible Phase Transfer of Coordination Cages and Their Cargoes. *J. Am. Chem. Soc.* **2018**, *140*, 14770−14776.

https://dx.doi.org/10.1021/jacs.0c02444
J. Am. Chem. Soc. 2020, 142, 7749−7753